The Astrophysical Journal, 632:49–57, 2005 October 10

BIMODAL COLOR DISTRIBUTION IN HIERARCHICAL GALAXY FORMATION

N. Menci, A. Fontana, E. Giallongo, and S. Salimbeni
INAF–Osservatorio Astronomico di Roma, Via di Frascati 33, I-00040 Monteporzio, Italy
Received 2005 February 4; accepted 2005 June 15

ABSTRACT

We show how the observed bimodality in the color distribution of galaxies can be explained in the framework of the hierarchical clustering picture in terms of the interplay between the properties of the merging histories and the feedback/star formation processes in the progenitors of local galaxies. Using a semianalytic model of hierarchical galaxy formation, we compute the color distributions of galaxies with different luminosities and compare them with the observations. Our fiducial model matches the fundamental properties of the observed distributions, namely: (1) the distribution of objects brighter than $M_r \lesssim -18$ is clearly bimodal, with a fraction of red objects increasing with luminosity; (2) for objects brighter than $M_r \lesssim -21$, the color distribution is dominated by red objects with color $u - r \approx 2.2$–2.4; (3) the spread on the distribution of the red population is smaller than that of the blue population; (4) the fraction of red galaxies is larger in denser environments, even for low-luminosity objects; and (5) the bimodality in the distribution persists up to $z \approx 1.5$. We discuss the role of the different physical processes included in the model in producing the above results.

Subject headings: cosmology: theory — galaxies: evolution — galaxies: formation — galaxies: high-redshift

Online material: color figure

1. INTRODUCTION

Recent observations indicate that the color function of galaxies at low redshift is characterized by a bimodal distribution (Strateva et al. 2001; Baldry et al. 2004), which defines two classes of galaxies: a red population, consisting mostly of non–star-forming galaxies that have formed most of their stellar mass at high redshift z; and a blue population, consisting of galaxies that are actively forming stars. The fraction of galaxies belonging to the red population grows with the luminosity L, being smaller than the blue fraction for $M_r > -19.5$ and dominating the distribution for $M_r > -21$. There is also a clear dependence on the galaxy environment, since red galaxies typically populate the overdense regions (Balogh et al. 2004). The bimodal galaxy distribution is present at least up to $z \approx 1$–2 (Bell et al. 2004; Giallongo et al. 2005).

Such a sharp, distinctive feature of the galactic population must constitute a powerful constraint to the galaxy formation models aiming at deriving the galactic properties "ab initio." These connect the formation of stars in progenitor dark matter (DM) halos (formed from the collapse of overdense regions in the primordial density field) with the assemblage of galaxies through repeated merging events involving the DM halos.

Such semianalytic models (SAMs), introduced by Kauffman et al. (1993) and Cole et al. (1994), have been greatly improved (Cole et al. 2000; Somerville & Primack 1999) also through the inclusion of starbursts driven by merging (Somerville et al. 2001; Menci et al. 2002) and flyby events (Menci et al. 2004) between satellite galaxies (see also Okamoto & Nagashima 2003). Recently, hydrodynamic simulations have also been able to provide independent insight into galaxy evolution on a cosmological scale (Nagamine et al. 2004, 2005; Davé et al. 2005). Although differences exist among these models, they are now in overall agreement not only with the local properties of galaxies but also with their statistical properties at high redshifts both in the K band (probing the total stellar mass assembled in galaxies) and in the B and UV bands (probing the star formation rate).

According to these models, the tendency of massive galaxies to be red and old, and of the low-mass ones to be bluer and star-forming, is a natural outcome of the hierarchical scenarios. Indeed, the progenitors of present-day massive galaxies formed in biased, high-density regions that collapsed at higher z and contained denser gas. Conversely, feedback effects are mostly effective at prolonging the active phase of star formation at low masses (typically below $\sim 10^{11}$–$10^{12}\ M_\odot$).

However, the existence of a clear bimodality in the galaxy color distribution constitutes a finer probe for the physical processes included in the models, since it suggests a dichotomy in the star formation histories of galaxies that should be originated by deep, fundamental properties of the galaxy formation process.

Here we investigate in detail whether the above qualitative trend of the hierarchical models may provide a bimodal color distribution in *quantitative* agreement with the observations. To this aim, we derive in § 2 the color distribution of galaxies as a function of their luminosity from a Monte Carlo version of the SAM model of Menci et al. (2004) and compare in § 3 the results with the observed distributions. In § 4 we discuss the physical origin of the bimodal distribution in hierarchical scenarios, as it emerges from our results.

2. THE MODEL

As a baseline, we adopt the SAM described in Menci et al. (2002, 2004); this connects the baryonic processes (gas cooling, star formation, and supernova feedback) to the merging histories of the DM halos and of the galactic subhalos there contained following the canonical recipes adopted by SAMs. Starbursts triggered by galaxy interactions (flyby and merging events) in common DM halos are also included as described in Menci et al. (2004). However, several changes have been made in both the DM and the baryonic sector of our model with respect to our previous papers. We describe such changes in turn.

2.1. *The Dark Matter Merging Trees*

To derive the whole color distribution we run a Monte Carlo version of our SAM, where many realizations of the merging histories of present-day DM halos (with different final masses) are drawn by extracting merging probabilities according to the

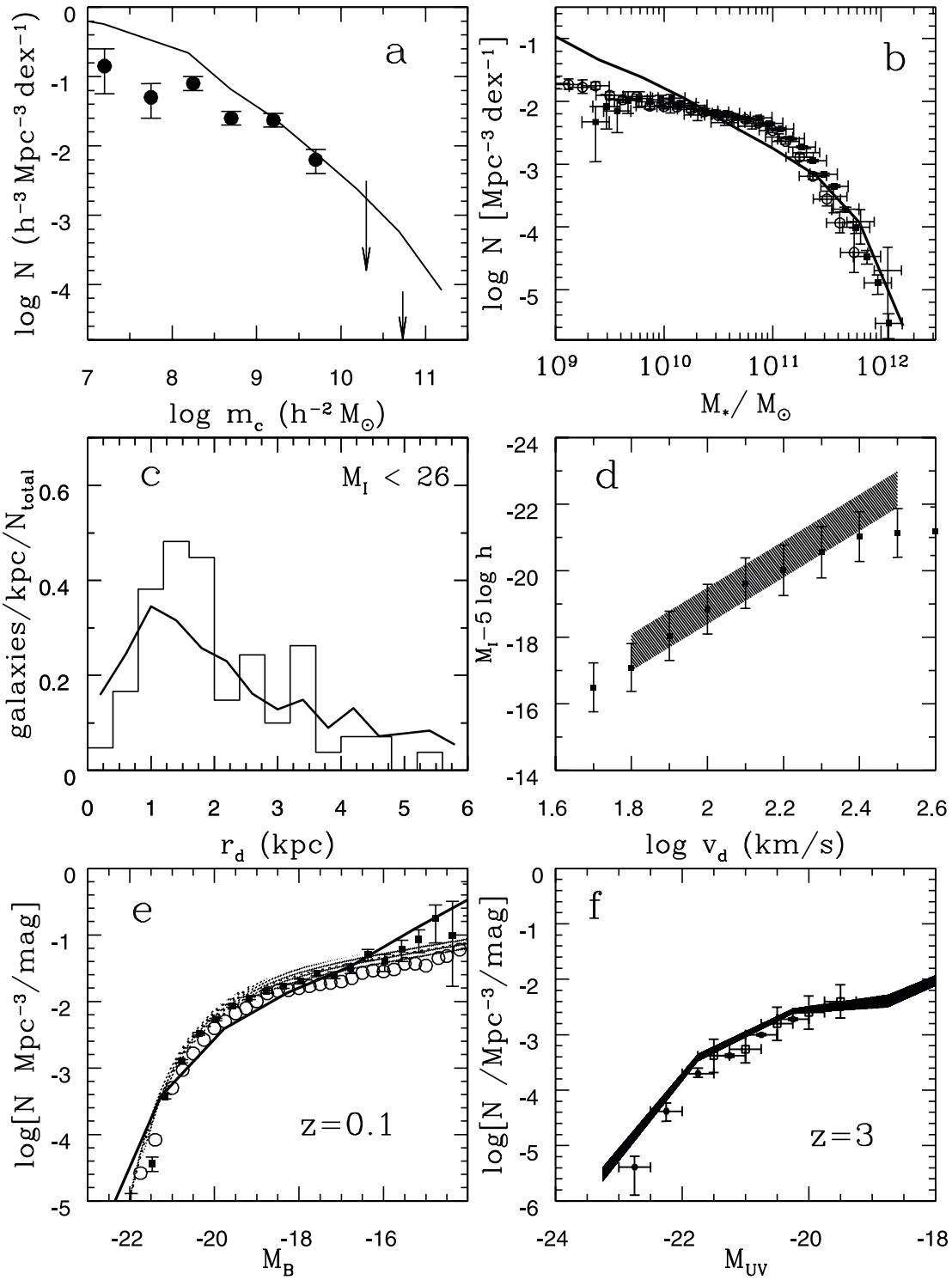

FIG. 1.—(*a*) Mass distribution of cold gas compared with the observed H I mass function, taken from Zwaan et al. (1997). The arrows show upper limits from the Arecibo surveys (see Schneider 1997). Note that the observed mass in H I constitutes a lower limit for m_c, since part of the cold gas is not in the form of H I. (*b*) Comparison of the local stellar mass distribution with the data from the Two Degree Field (2dF) survey (Cole et al. 2001; *filled squares*) and from the 2MASS survey (Bell et al. 2004; *open circles*). (*c*) Distribution of disk sizes (exponential scale lengths) from our model compared with the data obtained by Giallongo et al. (2000; *histogram*) for $M_I \leq 26$ galaxies in the Hubble and New Technology Telescope Deep Fields at $z = 0.4-0.7$. (*d*) The Tully-Fisher relation from our model (*squares*) with the 1 σ variance (*error bars*); the shaded region represents the region of the M_I-v plane spanned by the observations (Mathewson et al. 1992; Willick et al. 1996; Giovanelli et al. 1997). (*e*) The local *B*-band luminosity function from our model (*solid line*), assuming a Galactic dust extinction curve. The shaded area corresponds to the LF measured by the SDSS (Blanton et al. 2001), and the circles to the data from the 2dF Galaxy Redshift Survey (2dFGRS; Madgwick et al. 2002). We also show as filled squares the data from Zucca et al. (1997). (*f*) The UV luminosity function from our model; the shaded area represent the uncertainty in the model results due to assuming different extinction curves (SMC, Galactic, and Calzetti 1997). The spectroscopic (*filled squares*) and the photometric (*open squares*) data are from Steidel et al. (1999).

extended Press-Schechter (1974) theory (Bond et al. 1991; Lacey & Cole 1993). To generate the merging trees, we adopt the same algorithm described in Cole et al. (2000), with a grid of 25 final DM masses ranging from 3.16×10^9 to 1.8×10^{15} $M_\odot$ with equally spaced logarithmic values and a mass resolution of 5×10^7 $M_\odot$; a total of 100 realizations are drawn for each final DM mass. The evolution of DM halos described above is connected to the processes involving the baryons as described below.

2.2. *The Radiative Cooling*

The mass m_c of cooled gas in a disk with radius r_d and rotation velocity v_d is derived (Menci et al. 2002; Somerville & Primack 1999) by computing, for each time step, the increment in the cooling radius Δr_c of the central galaxy in all the DM halos. The corresponding increment of mass of the cooled gas is $\Delta m_c = 4\pi r_c^2 \rho_g(r_c)\Delta r_c$, assuming a simple isothermal gas density profile $\rho_g(r) \propto r^{-2}$. The normalization is set to recover the hot gas mass when the density profile is integrated over the volume. After merging events, we determine whether the mass of the largest progenitor m_1 comprises less than a fraction (1/2) of the post-merger mass (as in Somerville & Primack 1999); if this is the case (i.e., the merging partners have comparable masses), we reset the cooling time and cooling radius to zero (as suggested by recent, aimed hydrodynamic simulation of major galaxy merging; see Cox et al. 2004), and the gas is reheated to the virial temperature of the DM halo. The introduction of such a process suppresses the cooling in the massive halos, which undergo a larger number of such major merging events compared to low-mass halos. In addition, the steepness of the faint-end slope of the luminosity function (LF; see § 2.5 and Fig. 1) may help to account for the nonexistence of extremely bright ("monster") galaxies (see Benson et al. 2003). See also § 4 for a discussion on this point.

2.3. *The Star Formation Law and the Supernovae Feedback*

As for the star formation, we assume the canonical Schmidt form $\dot m_* = m_c/(q\tau_d)$, where $\tau_d \equiv r_d/v_d$ and q is left as a free parameter. At each time step, the mass Δm_h returned from the cold gas content of the disk to the hot gas phase due to supernovae (SNe) activity is estimated from canonical energy balance arguments (Kauffman 1996; Kauffmann & Charlot 1998; see also Dekel & Birnboim 2005) as $\Delta m_h = E_{\rm SN}\epsilon_0\eta_0\Delta m_*/v_c^2$, where Δm_* is the mass of stars formed in the time step, $\eta \approx (3\text{–}5)\times10^{-3}$ $M_\odot^{-1}$ is the number of SNe per unit solar mass (depending on the assumed initial mass function [IMF]), $E_{\rm SN} = 10^{51}$ ergs is the energy of ejecta of each SN, and v_c is the circular velocity of the galactic halo; $\epsilon_0 = 0.01\text{–}0.5$ is the efficiency of the energy transfer to the cold interstellar gas. The above mass Δm_h is made available for cooling at the next time step. The model-free parameters $q = 30$ and $\epsilon_0 = 0.1$ are chosen to match the local B-band LF and the Tully-Fisher relation adopting a Salpeter IMF.

2.4. *The Properties of the Disks*

The above star formation law depends strongly on r_d entering the timescale τ_d. The disk radius, $r_d = r_v g(v_c)$, is related to the DM virial radius r_v by the function $g(v_c)$ accounting for the properties of the disk; we adopt as our fiducial choice the model by Mo et al. (1998), which yields $g(v_c) \approx (\lambda/\sqrt{2})[j_d/(m_c/m)]\, f_c(v_c)^{-1/2} f_R(v)$, where we take for the DM spin parameter the average value $\lambda = 0.05$, while the ratio of the gas to DM angular momentum is kept to $j_d = 0.05$ as in Mo et al. (1998). The slowly varying functions f_c and f_R account for the gas density profile and for the self-gravity of the disk: the former is assumed to have the form given by Navarro et al. (1997); the concentration parameter entering their profile depends on the mass and is computed following the procedure given in the appendix of the above paper. The disk circular velocity v_d is computed according to the rotation curves in Mo et al. (1998) at a distance $3r_d$ from the disk center.

Note that our specific expression for $g(v)$ yields a star formation timescale $\tau_d \propto m/m_c$ and hence appreciably affects the star formation in the most massive halo where $\dot m_*$ is not effectively balanced by supernovae feedback. In particular, such halos are characterized by a larger $\dot m_*$ at high redshifts (where rapid cooling yields larger m_c/m ratios), which implies faster consumption of cold gas; at low-z, conversely, the longer star formation timescales due to the low m_c/m ratio inhibits the formation of stars in galaxies within massive DM halos.

2.5. *Testing the Model*

We summarize in Figure 1 some results of the model obtained for our fiducial choice of cosmological parameters: $\Omega_0 = 0.3$, $\Omega_\Lambda = 0.7$, $\Omega_b = 0.05$, and $H_0 = 70$ km s^{-1} Mpc^{-1}; the metallicity and the dust extinction are computed as in Menci et al. (2002), as well as the evolution of the stellar populations, with emission derived from synthetic spectral energy distributions (Bruzual & Charlot 1993), adopting a Salpeter IMF.

To test the consistency of our set of cooling, star formation, and feedback laws with the available observations, we first compare with the local observed distribution of cold gas, stars, disk sizes measured at low-z (Figs. 1*a*–1*c*), and with the Tully-Fisher relation in the I band (Fig. 1*d*). Then we compare with the B band (at low z) and the UV (at high z) luminosity functions (Figs. 1*e* and 1*f*) to show that the instantaneous star formation implemented in the model is consistent with observations over a wide range of cosmic times.

Note that the luminosity functions tend to overestimate the number of faint galaxies, a long-standing problem of hierarchical models; although this could be alleviated by increasing the v-dependence of the supernovae feedback, we prefer to keep the scaling of Δm_h to the relation $\Delta m_h \sim v_c^{-2}$ derived from the energy balance argument (see § 2.3) in order to keep the number of free parameters as low as possible; in addition, increasing the exponent of the above relation would worsen the agreement with the Tully-Fisher relation. However, we focus on the color distribution of relatively bright galaxies where the predicted and the observed luminosity function are still in good agreement.

The agreement of our model with the stellar mass functions up to $z \approx 1.5$ and with the K-band luminosity functions and counts up to the $z \approx 2$ is unchanged with respect to Menci et al. (2004).

3. RESULTS

3.1. *Bimodal Color Distribution at Low and High Redshift*

Here we present the color distributions of galaxies resulting from our model and compare them with the most distinctive observational results; these concern the dependence of the local color distributions on the galaxy luminosity and on the environment, and the persistence of the bimodal shape at higher z.

As for the former, we compare in Figure 2 the color distribution resulting from our model for different luminosity bins with the Gaussian fit to the observational points from the Sloan Digital Sky Survey (SDSS), given in Baldry et al. (2004) for the $u - r$ colors; details on the SDSS u and r bands are given by the above authors. We show our results for three kinds of dust extinction laws (SMC, Galactic, and Calzetti 1997); the corresponding color distributions are almost identical.

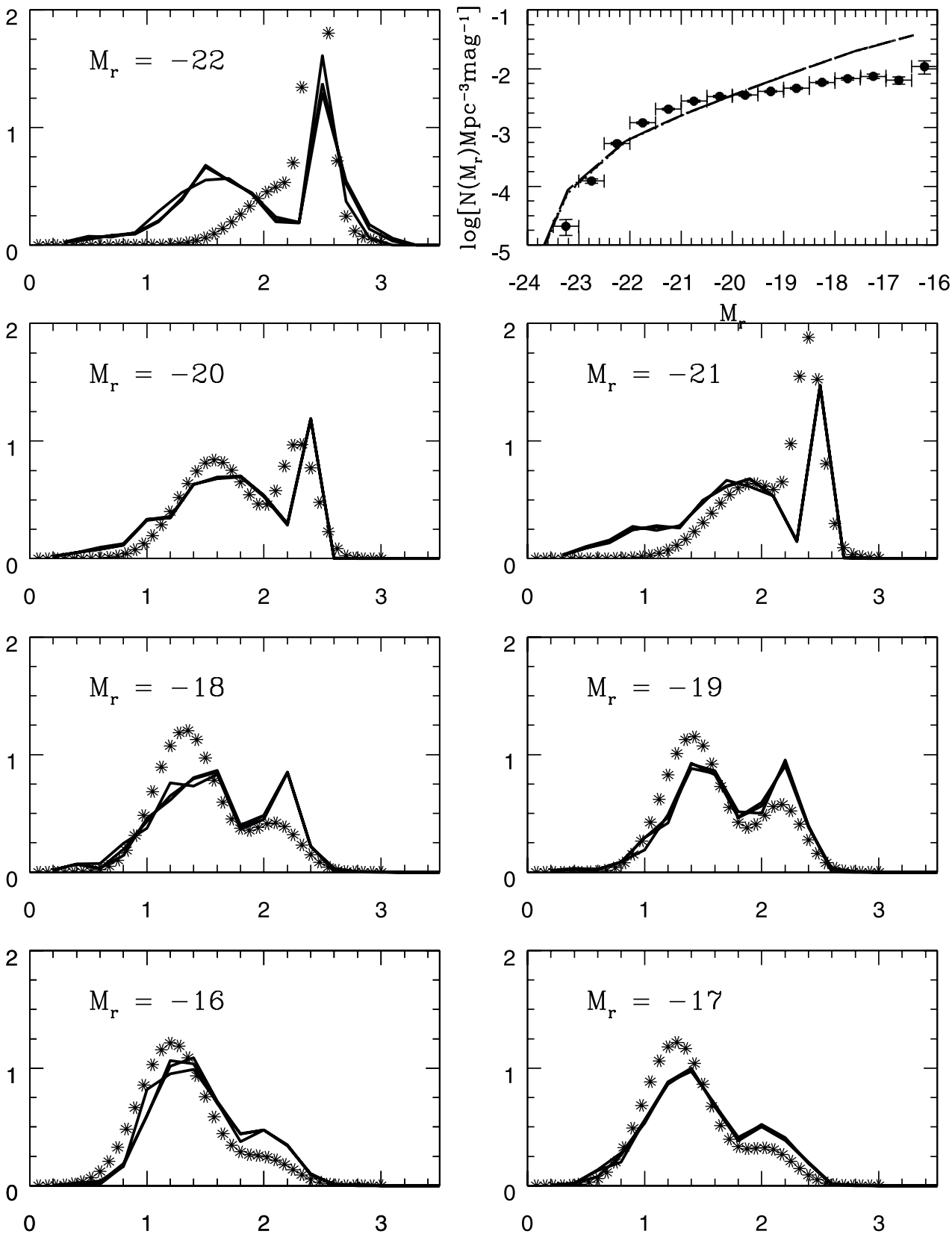

FIG. 2.—Predicted rest-frame $u - r$ color distributions (*thick lines*) for different dust extinction laws compared with the Gaussian fit to the SDSS data (from Baldry et al. 2004; *stars*) for different magnitude bins. The distributions are normalized to the total number of galaxies in the magnitude bin; the normalization of the data and of the model predictions are given by the *r*-band LFs shown in the top right panel. The typical size of error bars is shown in Fig. 6.

The plot shows that hierarchical galaxy formation may indeed produce a bimodal color distribution, with the fraction of red galaxies growing with increasing luminosities as observed. The color ($u - r \approx 2$) that marks the transition between the two populations is in good agreement with the observed distributions. In addition, the model naturally yields the correct behavior of the spread, the latter being $\approx$3 times larger for the blue population. Note, however, that the model predicts the existence of a residual fraction of blue, bright ($M_r \lesssim -22$) objects. Such an excess could be alleviated by including the feedback from active galactic nuclei (AGNs) in the SAMs; indeed, in our model, no feedback of this kind has been implemented. This shows that, although AGNs might appreciably contribute to suppress star formation in part of the massive galaxy population, they are not the origin of the observed bimodality in the color distribution, whose essential features are captured by our SAM.

We checked the robustness of our predictions against changes in the free parameters of our model, within the limits allowed by the simultaneous matching of the Tully-Fisher relation and of the *B*- and UV-band luminosity functions. We find that the main features of our models remain stable against most of these variations, although the quantitative details are sensitive to the parameter choice. For instance, increasing the feedback parameter ϵ_0 leads to a reddening of $\approx$0.3 of the transition color that marks the partition between the red and blue populations. Increasing the star formation timescale within the limit $q \lesssim 60$ results in a progressively less pronounced bimodality and in more concentrated distributions around the same average color. We have checked that changing the normalization of the dust absorption or of the stellar yield (and hence of metallicity, implemented as described in Menci et al. 2002) does not affect appreciably our color distributions if such normalizations are chosen so as to match the *B*- and UV-band luminosity functions from $z = 0$ to 3. The only significant exception to this rule is the critical dependence on the prescriptions for the star formation laws: we return to this issue in § 3.2.

The environmental dependence of our color distributions is shown in Figure 3, where we compare with the SDSS data from Balogh et al. (2004); for a given luminosity range, these have been binned according to different environmental densities defined inside a given region around the fifth brightest galaxy. Since our SAM does not include any spatial information, we cannot perform a fully consistent comparison, so we proceed as follows. We focus on the less luminous bin $-18 < M_r < -19$ considered by Balogh et al. (2004), since the environmental effects produce the most dramatic changes in the color distribution at low luminosities. Then we select the less massive and the most massive parent DM halos in our Monte Carlo run and compare the color distributions of the galaxies contained in such environments with the less and the most dense environment considered in Balogh et al. (2004). The highest density environment considered by Balogh et al. (2004) corresponds to the core of rich clusters of galaxies, roughly consistent with our most massive DM parent halo at $z = 0$, which has a mass $1.8 \times 10^{15}\ M_\odot$; as for the underdense regions, we select from our Monte Carlo the less dense environment (the less massive parent halo at $z = 0$) containing a galaxy with magnitude in the considered range; the corresponding lower density environment in Balogh et al. (2004) has a projected surface density of 0.1 Mpc^{-2}.

Within the limits of our comparison, the model correctly reproduces the observed shift of the distribution toward redder colors when denser environments are considered. Indeed, the environmental dependence appearing in Figure 3 is stronger than the luminosity dependence; in fact, in the densest environments (originated from the most biased regions of the primordial field) the distribution is entirely skewed toward red ($u - r > 2.3$) colors, even when low luminosities ($-18 < M_r < -19$) are considered. A similar agreement holds for other luminosity ranges; in particular, the high-luminosity range ($M_r \lesssim -21$) is dominated by red galaxies in all environments.

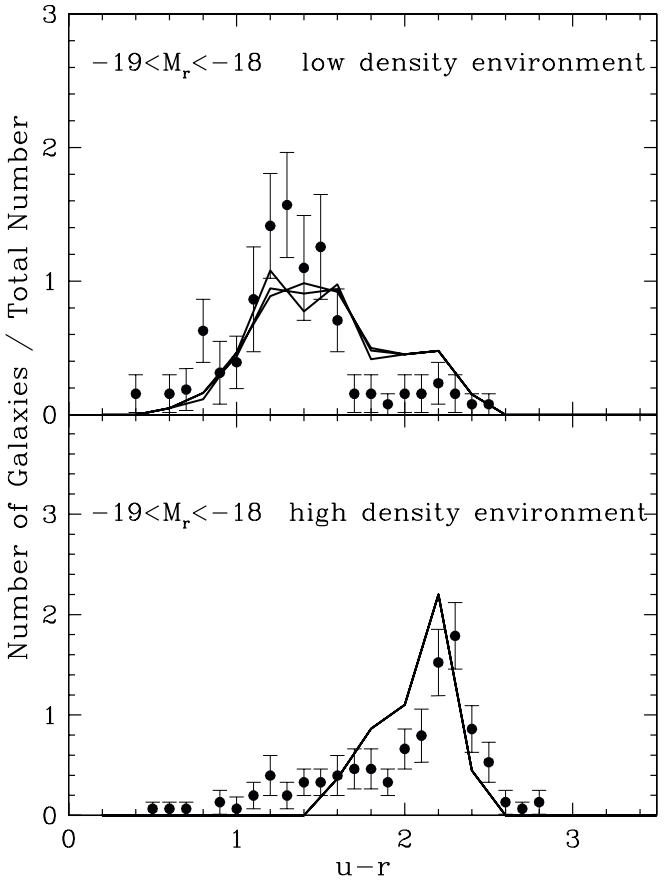

FIG. 3.—Dependence of the $u - r$ color distribution on the environment plotted for galaxies in the bin $-18 < M_r < -19$ to allow a comparison with the SDSS distribution (*dots*; from Balogh et al. 2004) in lower (*top*) and highest density (*bottom*) environments where the considered galaxies are found (see text). The distributions have been normalized to yield unity when integrated over color.

Finally, we show in Figure 4 the model predictions at higher redshifts. At $z \approx 1$ we compare with data from Giallongo et al. (2005); their composite sample (see figure legend) covers a range spanning from UV down to the optical/IR wavelengths, with different depths reaching $m_{H_{AB}} = 26$ in the deepest field. The bimodal distribution computed from the model persists at $z \approx 1$, in agreement with observations (see also Bell et al. 2004); indeed, our model predicts the bimodality to be clearly present up to $z \approx 1.5$ (*dashed lines*).

3.2. *Star Formation Histories of Blue and Red Galaxies*

The individual star formation histories of the galaxies produced in our model provide a clear visualization of the evolutionary paths that led to the present-day red and blue populations. We show in Figure 5 a selection of individual star formation histories in our model, as obtained by summing over all the progenitor clumps that have merged to form galaxies of $M_r \simeq -20$ at $z = 0$. As expected, the histories of the blue galaxies extend to much lower redshift than the red one, resulting in their bluer colors. We also remark the large variety of histories corresponding the blue

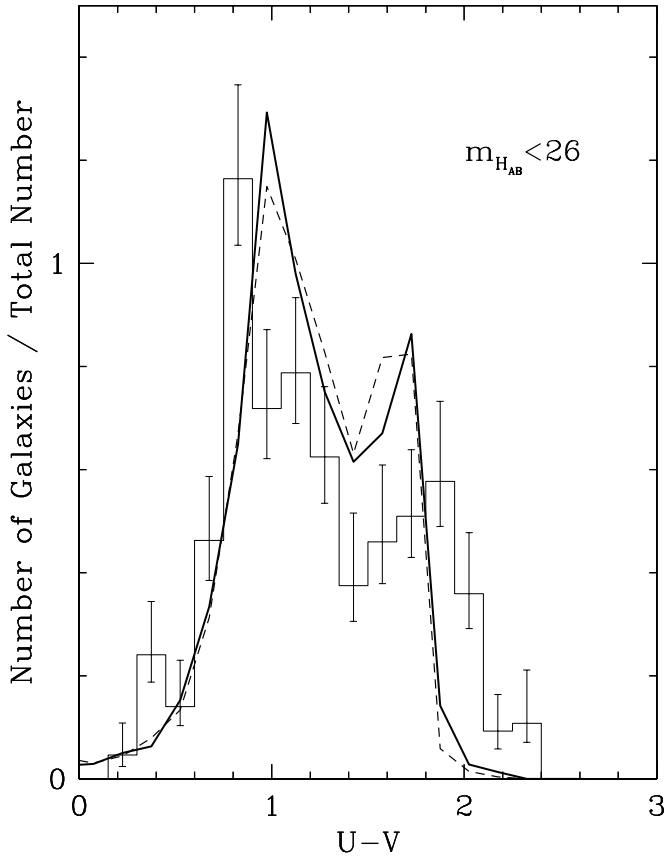

FIG. 4.—Plot of the $U - V$ color distribution at $0.8 < z < 1$ of $m_{H_{AB}} < 26$ galaxies in our model compared with the data by Giallongo et al. (2005) derived from a composite sample of galaxies including a portion of the K20 field (Cimatti et al. 2002), and the Hubble Deep Field–North, Hubble Deep Field–South, and Chandra Deep Field; the Poisson error in each color bin was computed adopting the recipe by Gehrels (1986), valid also for small numbers. We also show as a dashed curve the predicted color distribution at $z = 1.5$ for the same magnitude limit.

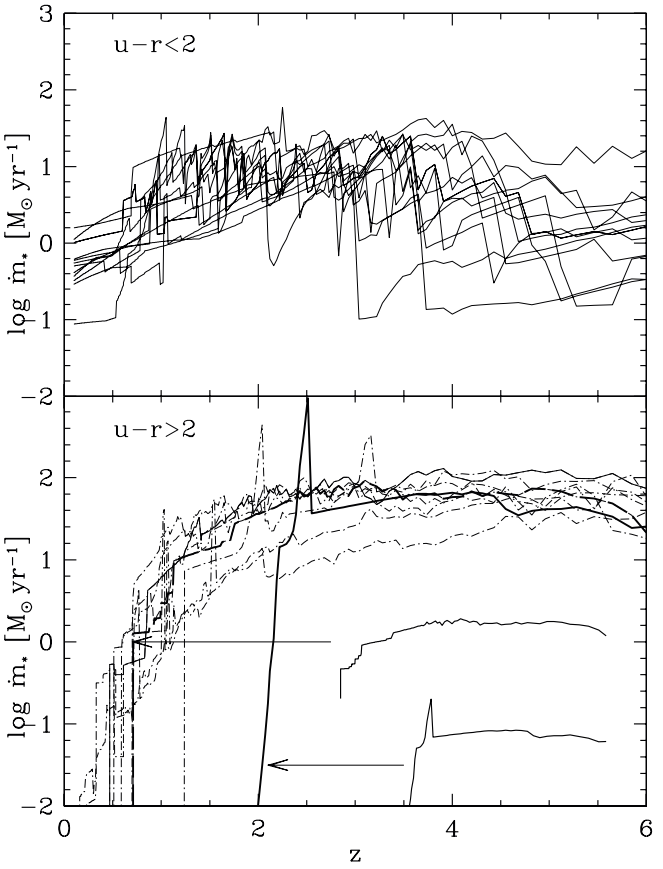

FIG. 5.—Star formation histories drawn from Monte Carlo realizations of galaxies that, at $z = 0$, have luminosities in the range $-19.5 \leq M_r \leq -20.5$. Each curve represents the sum of the $\dot{m}_*$ in all the progenitor clumps (at any given z) of galaxies belonging (at $z = 0$) to the blue ($u - r < 2$; *top*) and red ($u - r > 2$; *bottom*) populations. Two star formation histories relevant to our discussion (see text) are highlighted by thick curves (*solid and dashed lines*) and evidenced by the insets in the lower part of the plot.

population that is at the origin of the larger scatter observed in their color distributions at $z \approx 0$. On the other hand, the star formation histories of red galaxies are more similar (resulting in smaller scatter of the color function at $z \approx 0$; see Fig. 2), with large values of $\dot{m}_*$ at $z \gtrsim 2.5$; note that such histories are broadly peaked at $z \approx 4$–5 and sharply decline at $z \lesssim 2$, while the histories leading to blue local galaxies typically reach their maximum at $z \approx 2$–3, since at high-z the star formation is effectively suppressed by supernovae feedback (see § 5).

Note that bursts do not seem to constitute the physical origin of the bimodality in the color distribution at $z \approx 0$. Indeed, the red side of the population is mostly contributed by galaxies with smoothly evolving $\dot{m}_*$ (like that represented by the thick dashed line in the bottom panel of Fig. 5), although several histories are characterized by major bursts, such as the extreme star formation history (marked by the thick solid line in the bottom panel), which has undergone a major burst at $z \approx 2.5$. On the other hand, bursts seem to be crucial in providing extremely red objects (EROs) already at high $z \gtrsim 1.5$, as shown again by the history marked by the thick solid line; see also the other history characterized by a major burst at $z \approx 2$ and by a drop of $\dot{m}_*$ at $z \gtrsim 1.3$.

We checked that switching off starbursts triggered by encounters does not affect appreciably the bimodality of our color distribution at $z \approx 0$; this is consistent with our previous results (Menci et al. 2004), which showed such events to alter mainly the properties of large-mass galaxies at $z \gtrsim 1$ without affecting the local distributions. The above conclusion is confirmed by the observation that galaxies residing in dense environments are characterized by red colors at $z = 0$ even if their luminosity/mass is moderate (see Fig. 4); such a property is difficult to explain only in terms of starbursts triggered by major mergings, since the merging probability of small-mass galaxies in high-density environments is strongly suppressed not only by their small cross section but also by the large velocity dispersion characteristic of galaxy clusters.

We now proceed to discuss the fundamental processes that are at the basis of the dichotomy between the star formation histories shown in the top and bottom panels of Figure 5, leading to the bimodal color distribution at low z.

4. HIERARCHICAL CLUSTERING AND THE ORIGIN OF BIMODALITY

In hierarchical models, the scatter in the colors of galaxies with given final DM mass is due to the different realizations of the merging histories that lead to the considered mass; these ultimately trace back to the properties of the primordial density perturbations field where the galaxy progenitors first formed.

In such a context, a correlation between the galaxy mass and the color is naturally predicted; in fact, the star formation in progenitor clumps later included into massive galaxies is peaked at higher redshift compared to that taking place in progenitors of

small-mass galaxies, since the former form in the biased, high-density regions of the density field, collapsing at higher z and containing denser gas. However, the absence of a typical mass scale in the progenitor distribution would not produce by itself a sharp transition in the star formation rate like that needed to originate the bimodal color distribution.

A nongravitational mass scale is naturally introduced in the star formation properties of different merging histories by the SNe feedback (as suggested by Dekel & Silk 1986; see Dekel & Birnboim 2005 and references therein). In low-mass galactic halos such feedback rapidly reheats the cold gas not converted into stars, resulting in a self-regulated regime with $\Delta m_* \sim \Delta m_c$, where Δm_c is the mass of gas cooled in the time step. The upper mass limit for such a regime to be effective can thus be estimated from $v_c^2 \lesssim \epsilon_0 \eta E_{\rm SN} \approx 100$ km s^{-1} (see § 1; for a more detailed derivation, see Dekel & Birnboim 2005), which at high $z \approx 4$–5 corresponds to DM masses as low as $m_0 \approx 10^9\ M_\odot$. Thus, in progenitor halos with $m < m_0$ the star formation at high z is self-regulated and is forced to remain below the limit set by the equilibrium between the feedback and the star formation (White & Frenk 1991); on the other hand, in progenitors with $m > m_0$ the cold gas reservoir may grow (up to the maximal value Ω_b/Ω) at high z, and the star formation rate is limited only by the efficiency of cold gas conversion into stars (determined by the timescale τ_d).

Thus, hierarchical clustering naturally predicts (1) the star formation in progenitor clumps later included into massive galaxies to peak at higher redshift compared to that taking place in progenitors of small-mass galaxies and (2) the existence of a mass threshold m_0 below which the cold gas content of the DM clumps at high z is effectively reheated and the star formation is self-regulated. Such generic features are in qualitative agreement with the observation that bright galaxies are typically redder (de Vaucouleurs 1961; Bower et al. 1992).

In our model, the above two points combine with (3) a star formation efficiency that enforces the partition between gas-rich and gas-poor systems, above and below the threshold m_0. Specifically, we adopt $\tau_d \propto m/m_c$, derived from the disk model developed by Mo et al. (1998; as described in § 2).

In fact, at high z, the cold gas reservoir of progenitors clumps with $m < m_0$ is continuously depleted by effective feedback, as discussed above; this increases the timescale $\tau_d \propto m/m_c$, thus suppressing star formation and avoiding the sudden conversion of cold gas into stars. At later cosmic times, as the progenitor masses grow above the threshold m_0, cold gas begins to accumulate in the progenitor clumps and is made available for star formation, which continues down to low redshifts. Such smooth star formation histories (Fig. 5, *top panel*) lead to the local faint blue population.

On the other hand, in progenitor clumps with $m > m_0$ at high-z the cold gas is not effectively reheated; thus, the rapid cooling taking place at high-z leads to large m_c/m ratios, which shorten the star formation timescale. The cold gas is rapidly converted into stars and begins to exhaust at $z \lesssim 2$ (see Fig. 5); at later times the star formation is further suppressed, since now such galaxies have low m_c/m ratios. Thereafter, such galaxies undergo an almost quiescent phase characterized by a fast drop of $\dot{m}_*$; such histories are typical of massive galaxies and of galaxies forming in biased regions of the primordial density field (which later become the galaxy environment) and originate the red population at $z \approx 0$.

The more effective the star formation in high-z, gas-rich halos, the sharper the transition between the feedback-regulated regime and the supply-limited regime. In fact, when we adopt a star formation timescale not explicitly depending on m_c/m (as in most current SAMs), we obtain a smooth (nonbimodal) color distribution; this is shown in Figure 6, where the color distribution from our model is compared with that obtained on adopting a fixed value for the ratio $m_c/m = 0.05$ (the average value in Mo et al. 1998) in the expression for the function $g(v)$ defined in § 2. Note that this model still predicts a correlation between the color and the luminosity of present-day galaxies: as we discussed above, this is indeed a generic feature of hierarchical scenarios. In our fiducial model, we achieve a redder color in an appreciable fraction of galaxies compared to the model with fixed m_c/m.

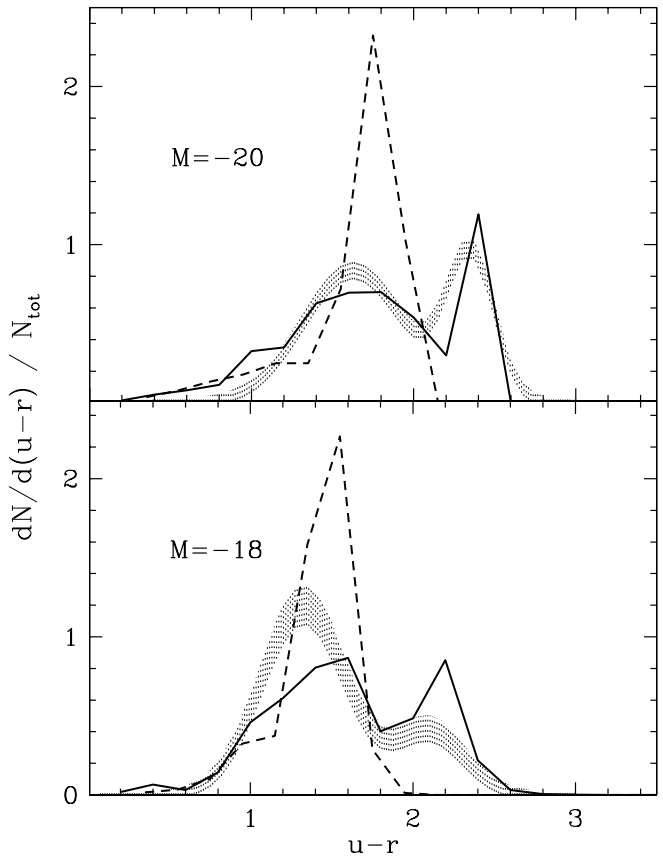

FIG. 6.—Color distribution of our fiducial model (*solid line*)—i.e., star formation timescale $\tau_d \propto m/m_c$ derived from the disk model developed by Mo et al. (1998)—compared with that obtained by the model assuming a constant ratio $m_c/m = 0.05$ (*dashed lines*). The shaded area represents the uncertainty in the Gaussian fits to the SDSS data (Baldry et al. 2004).

To summarize, in our model the star formation in massive halos at low redshift is suppressed by three concurring processes: (1) at high-z, the rapid conversion of gas into stars, enhanced by our star formation timescale $\tau_d \propto m/m_c$, leads to a fast exhaustion of the cold gas reservoir; (2) at $z \lesssim 2$, the cold gas reservoir of massive galaxies is depleted by major merging events (see § 2); and (3) as a consequence of conditions (1) and (2), the ratio m_c/m in such galaxies is particularly low, leading to a longer star formation timescale $\tau_d \propto m/m_c$, which further suppresses star formation.

It must be emphasized that results similar to our model might be obtained by any mechanism enforcing the dependence of $\dot{m}_*$ on the cold gas accretion (such as the cold streams discussed by Dekel & Birnboim 2005).

Thus, the origin of bimodality is connected to the interplay between the properties of the merging histories involving the progenitors of local galaxies and the feedback/star formation process. To further test such a picture, we proceed as follows.

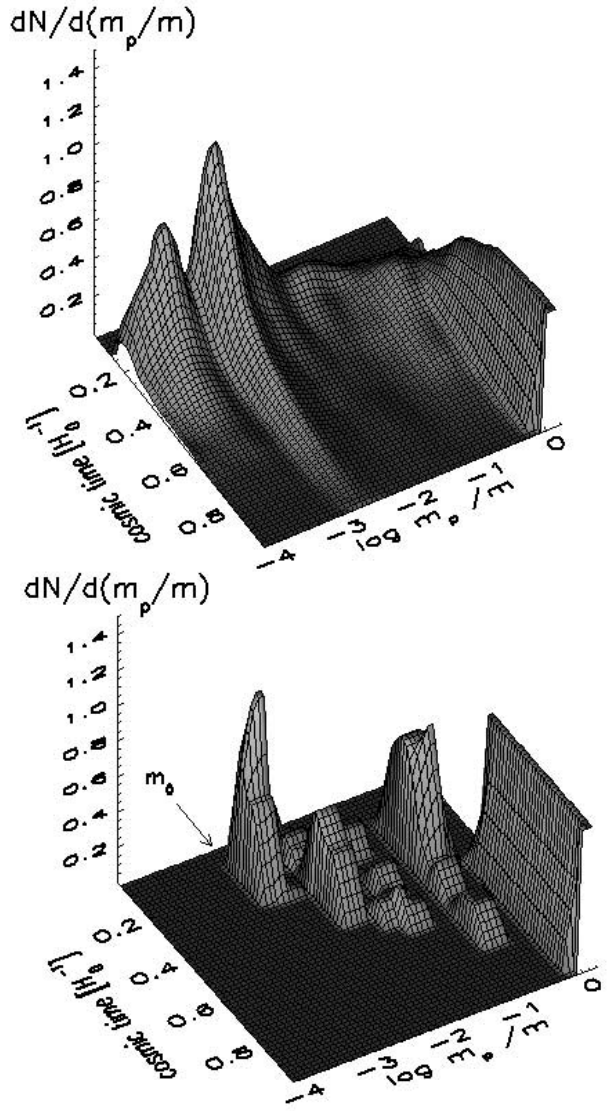

FIG. 7.—Distribution $dN/d(m_p/m)$ of progenitors of local galaxies with luminosity $-19.75 < M_r < -20.25$ as a function of the progenitor mass m_p (normalized to the final mass of the galaxy m) and of the cosmic time. The top panel refers to local galaxies with blue ($u - r < 2$) color, and the bottom panel refers to the red ones ($u - r \geq 2$). Time is in units of $1/H_0$; in such units, $t = 0.1$ corresponds to $z = 4.2$, and $t = 0.4$ corresponds to $z = 1$. [*See the electronic edition of the Journal for a color version of this figure.*]

We focus on the merging histories of galaxies with luminosity (at $z = 0$) in the bin centered at $M_r = -20$ (so that the considered galaxies have similar total mass $m \approx 10^{12}\ M_\odot$), and we select the galaxies belonging to the blue and red local populations. We then compute the mass distribution of the progenitors of the (locally) red and blue galaxies, separately, which are shown at different redshifts in Figure 7.

As expected in our picture, the two classes of merging histories are qualitatively different. At the highest redshifts the mass distribution of the progenitors of the (present-day) red galaxies is skewed toward larger masses compared with the blue ones, and they rapidly reach their final mass. Conversely, the merging histories of present-day blue galaxies are characterized by the infall of low-mass progenitors well below $z \approx 1$, leading to a refueling of gas over a longer cosmic time. Moreover, the existence of a low-mass threshold for the progenitors of the red objects (corresponding to the mass scale m_0) is clearly shown by the plot; the numerical value of m_0 obtained from the bottom panel in Figure 7 corresponds to the critical velocity of 100 km s^{-1} derived above by requiring the reheating from feedback to regulate the star formation rate.

This confirms our picture and reveals that the low-z colors of galaxies are the final result of a partition in the star formation histories of the progenitors occurring at high $z \approx 4$–5. Such a partition is originated by the properties of the DM density field, the existence of a mass threshold for self-regulating star formation, and a star formation efficiency that enforces the partition between gas-rich and gas-poor systems, above and below the threshold m_0.

5. SUMMARY AND CONCLUSIONS

We quantitatively showed how the observed properties of the bimodal color distribution of galaxies arises, in the framework of the hierarchical clustering picture, from the interplay between the properties of the merging histories involving the progenitors of local galaxies and the feedback/star formation process.

Our SAM successfully matches several fundamental properties of the galaxy color distribution: its bimodal shape at $z \approx 0$ defining two classes of objects whose partition occurs at $u - r \approx 2$, with a small spread in the distribution of red objects compared to the blue ones (Fig. 2); the luminosity dependence of the bimodal distribution, characterized by the red population growing with increasing L and dominating the distribution for $M_r \lesssim -21$ (Fig. 2); its environmental dependence (characterized by redder galaxies in denser environments), which overrides the luminosity dependence in the sense that even the color distribution of local faint galaxies ($-18 < M_r < -19$) is skewed toward red ($u - r \approx 2.2$) colors (Fig. 3) when only dense environments are considered; and the persistence of the bimodal distribution up to $z \approx 1.5$ (Fig. 4).

We have also shown that the two color populations result from two classes of star formation (Fig. 5) and merging histories as follows.

1. Merging histories leading to the local red population are characterized by a progenitor distribution skewed toward larger masses at high $z \approx 4$–5 (Fig. 7, *bottom panel*). In such progenitors, feedback is ineffective in reheating/expelling the cold gas content, and if the latter is rapidly converted into stars at $z \approx 4$–5, the main progenitors exhaust their cold gas reservoir at $z \approx 2$ (see Fig. 5) and thereafter undergo an almost quiescent phase characterized by a fast drop of $\dot{m}_*$. Massive galaxies and galaxies formed in a biased region of the primordial density field (which later become the galaxy environment) are preferentially assembled through the former kind of merging history. This straightforwardly explains the luminosity and environmental dependence of the color distribution.

2. Merging histories leading to the local blue population are characterized by a progenitor distribution dominated by small-mass progenitors (Fig. 7, *top panel*). There the star formation is self-regulated by feedback, which limits the cold gas content and is effective in prolonging the active phase of star formation. In addition, such merging histories are characterized by the infall of low-mass progenitors down to $z \approx 1$, resulting in a refueling of gas extended over a longer cosmic time. The corresponding star formation histories are illustrated in the top panel of Figure 5. Small-mass galaxies are generally built up through this evolutionary path.

Hierarchical clustering provides a framework for the rising of bimodality because of two natural features: (1) star formation histories of massive galaxies and of galaxies formed in biased,

high-density regions are peaked (on average) at higher z compared to lower mass galaxies; and (2) the existence of a nongravitational mass scale m_0 (whose value corresponding to $v \approx 100$ km s^{-1} is set by the supernovae feedback) such that for $m < m_0$ the star formation is self-regulated and the cold gas content is continuously depleted by effective feedback. These features are generic to most hierarchical clustering models and typically contribute to yield to a global color-magnitude relation where brighter galaxies tend to be redder.

Within such a framework, star formation laws, which enhance the gas consumption effects described above, are necessary to yield a bimodality in the color distribution of present-day galaxies. In particular, we have shown that enforcing the dependence of $\dot{m}_*$ on the cold gas accretion above the scaling $\dot{m}_* \propto m_c$ leads to a sharper partition in the star formation histories of clumps with progenitor masses above and below m_0. Thus, the bimodal color distribution of galaxies originates at high redshifts $z \approx 4$–5 during the formation and merging of their progenitors. This naturally explains the observed appearance of a bimodal distribution already at $z \approx 1.5$.

We thank A. Cavaliere, P. Salucci, and R. Somerville for useful discussions. We acknowledge grants from Ministero dell'Università e della Ricerca Scientifica e Tecnologica (MURST).

REFERENCES

Baldry, I. K., Glazebrook, K., Brinkmann, J., Zeljko, I., Lupton, R. H., Nichol, R. C., & Szalay, A. S. 2004, ApJ, 600, 681
Balogh, M. L., Baldry, I. K., Nichol, R. C., Miller, C., Bower, R., & Glazebrook, K. 2004, ApJ, 615, L101
Bell, E., Wolf, C., Meisenheimer, K., Rix, H.-W., Borch, A., Dye, S., Kleineinrich, M., & McIntosh, D. 2004, ApJ, 608, 752
Benson, A. J., Bower, R. G., Frenk, C. S., Lacey, C. G., Baugh, C. M., & Cole, S. 2003, ApJ, 599, 38
Blanton, M. R., et al. 2001, AJ, 121, 2358
Bond, J. R., Cole, S., Efstathiou, G., & Kaiser, N. 1991, ApJ, 379, 440
Bower, R. J., Lucey, J. R., & Ellis, R. S. 1992, MNRAS, 254, 601
Bruzual, A. G., & Charlot, S. 1993, ApJ, 405, 538
Calzetti, D. 1997, in AIP Conf. Proc. 408, The Ultraviolet Universe at Low and High Redshift: Probing the Progress of Galaxy Evolution, ed. W. H. Waller et al. (New York: AIP), 403
Cimatti, A., et al. 2002, A&A, 392, 395
Cole, S., Aragon-Salamanca, A., Frenk, C. S., Navarro, J. F., & Zepf, S. E. 1994, MNRAS, 271, 781
Cole, S., Lacey, C. G., Baugh, C. M., & Frenk, C. S. 2000, MNRAS, 319, 168
Cole, S., et al. 2001, MNRAS, 326, 255
Cox, T. J., Primack, J., Jonsson, P., & Somerville, R. S. 2004, ApJ, 607, L87
Davé, R. 2005, in Proc. IAU Symp. 216, Maps of the Cosmos, ed. M. Colless, L. Staveley-Smith, & R. Stathakis (Cambridge: Cambridge Univ. Press), in press
Dekel, A., & Birnboim, Y. 2005, ApJ, submitted (astro-ph/0412300)
Dekel, A., & Silk, J. 1986, ApJ, 303, 39
de Vaucouleurs, G. 1961, ApJS, 5, 233
Gehrels, N. 1986, ApJ, 303, 336
Giallongo, E., Menci, N., Poli, F., D'Odorico, S., & Fontana, A. 2000, ApJ, 530, L73
Giallongo, E., Salimbeni, S., Menci, N., Zamorani, G., Fontana, A., Dickinson, M., Cristiani, S., & Pozzetti, L. 2005, ApJ, 622, 116
Giovanelli, R., Haynes, M. P., da Costa, L. N., Freudling, W., Salzer, J. J., & Wegner, G. 1997, AJ, 113, 22
Kauffmann, G. 1996, MNRAS, 281, 475
Kauffmann, G., & Charlot, S. 1998, MNRAS, 294, 705
Kauffmann, G., White, S. D. M., & Guiderdoni, B. 1993, MNRAS, 264, 201
Lacey, C., & Cole, S. 1993, MNRAS, 262, 627
Madgwick, D. S., et al. 2002, MNRAS, 333, 133
Mathewson, D. S., Ford, V. L., & Buchhorn, M. 1992, ApJS, 81, 413
Menci, N., Cavaliere, A., Fontana, A., Giallongo, E., & Poli, F. 2002, ApJ, 575, 18
Menci, N., Cavaliere, A., Fontana, A., Giallongo, E., Poli, F., & Vittorini, V. 2004, ApJ, 604, 12
Mo, H. J., Mao, S., & White, S. D. M. 1998, MNRAS, 295, 319
Nagamine, K., Cen, R., Hernquist, L., Ostriker, J. P., & Springel, V. 2005, ApJ, 627, 608
Nagamine, K., Springel, V., Hernquist, L., & Machacek, M. 2004, MNRAS, 350, 385
Navarro, J. F., Frenk, C. S., & White, S. D. M. 1997, ApJ, 490, 493
Okamoto, T., & Nagashima, M. 2003, ApJ, 587, 500
Press, W. H., & Schechter, P. 1974, ApJ, 187, 425
Schneider, S. E. 1997, Publ. Astron. Soc. Australia, 14, 99
Somerville, R. S., & Primack, J. R. 1999, MNRAS, 310, 1087
Somerville, R. S., Primack, J. R., & Faber, S. M. 2001, MNRAS, 320, 504
Steidel, C. C., Adelberger, K. L., Giavalisco, M., Dickinson, M., & Pettini, M. 1999, ApJ, 519, 1
Strateva, I., et al. 2001, AJ, 122, 1861
White, S. D. M., & Frenk, C. S. 1991, ApJ, 379, 52
Willick, J. A., Courteau, S., Faber, S. M., Burstein, D., Dekel, A., & Kolatt, T. 1996, ApJ, 457, 460
Zucca, E., et al. 1997, A&A, 326, 477
Zwaan, M. A., Briggs, F. H., Sprayberry, D., & Sorar, E. 1997, ApJ, 490, 173